

If we eliminate the post-shock velocity, energy conservation can be rewritten as a purely thermodynamic relation known as the *Hugoniot* or *shock adiabat*.

$$h_2 - h_1 = (P_2 - P_1) \frac{(v_2 + v_1)}{2} \quad (6.18)$$

or

$$e_2 - e_1 = \frac{(P_2 + P_1)}{2} (v_1 - v_2) \quad (6.19)$$

From the previous discussion on chemical composition, we can write the enthalpy as a function of volume and pressure $h_2(v_2, P_2)$ since temperature is related to pressure and volume by

$$v_2 = \frac{R_2 T_2}{P_2} \quad (6.20)$$

From the definition of internal energy $e = h - Pv$, so $e_2 = e_2(P_2, v_2)$. In principle, this means we can solve

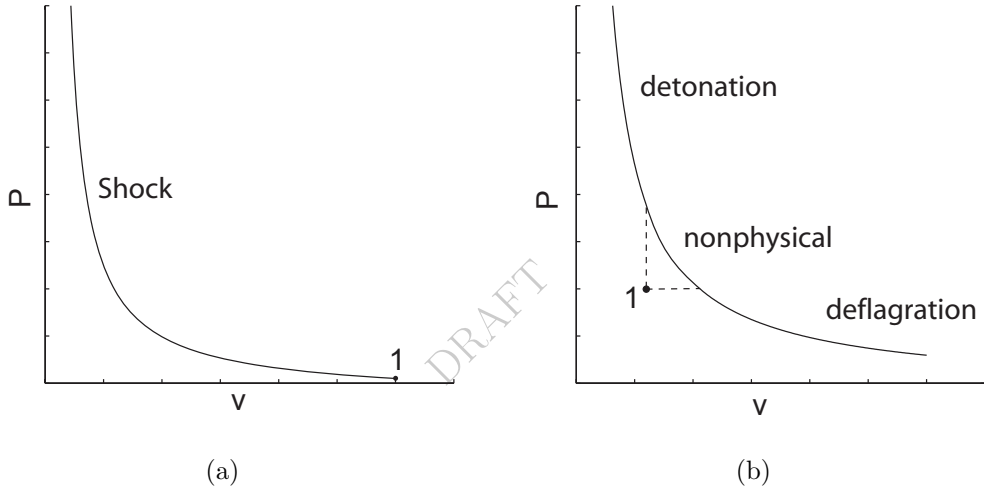


Figure 6.2: Hugoniots (a) Shock wave propagating in a non-exothermic mixture or a mixture with frozen composition. (b) Shock wave propagating in an exothermic mixture.

either (6.18) or (6.19) to obtain the locus of all possible downstream states $P_2(v_2)$ for a fixed upstream state. The result $P(v)$ is referred to as the Hugoniot curve or simply Hugoniot. For a frozen composition or an equilibrium composition in a non-exothermic mixture like air, Fig. 6.2a, the Hugoniot curve passes through the initial state. For an equilibrium composition in an exothermic mixture like hydrogen-air, Fig. 6.2b, the chemical energy release displaces the Hugoniot curve from the initial state. The Rayleigh line slope (6.17) is always negative and dictates that the portion of the Hugoniot curve between the dashed vertical and horizontal lines (Fig. 6.2b) is nonphysical. The nonphysical region divides the Hugoniot into two branches: the upper branch represents supersonic combustion waves or *detonations*, and the lower branch represents subsonic combustion waves or *deflagrations*. The properties of the detonation and deflagration branches are discussed in more detail in Section 6.5.

The advantage of using the Rayleigh line and Hugoniot formulation is that solutions of the jump conditions for a given shock speed can be graphically interpreted in P - v diagram as the intersection of the Hugoniot and a particular Rayleigh line. This is discussed in the next sections for shock and detonation waves.

See the following examples of Rayleigh and Hugoniot lines:
MATLAB Demos:

`demo_RH.m`, `demo_RH_air.m`, `demo_RH_air_eq.m`, `demo_RH_air_isentropes.m`, and `demo_RH_CJ_isentropes.m` Python Demos:
`demo_RH.py`, `demo_RH_air.py`, `demo_RH_air_eq.py`, `demo_RH_air_isentropes.py`

6.4 Shock Waves - Frozen and Equilibrium

Examples of the use of the Shock and Detonation Toolbox to find downstream states for shock waves in air are shown in Figure 6.3. The Rayleigh line and the Hugoniots are shown for two ranges of shock speed. For shock speeds less¹ than 1000 m/s (the Rayleigh line shown in Fig. 6.3a), the frozen and equilibrium Hugoniots are indistinguishable. At these shock speeds, only a small amount of dissociation occurs behind the shock front so that the composition is effectively frozen. Under these conditions, solutions to the shock jump conditions are only slightly different from the analytical results for constant specific heat ratio (perfect gas approximation) given in Appendix A.1. Fig. 6.3a was obtained using the MATLAB script `demo_RH_air`.

For shock speeds between 1000 m/s and 3500 m/s, Fig. 6.3b, the differences between frozen and equilibrium Hugoniot curves becomes increasing apparently with increasing pressure at state 2 corresponding to increasing shock speeds. Fig. 6.3b was obtained using the MATLAB script `demo_RH_air_eq.m`.

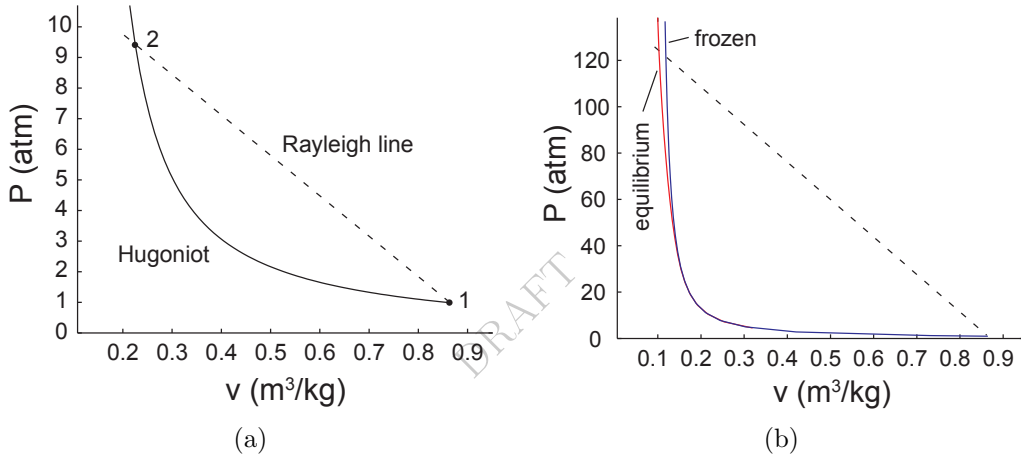


Figure 6.3: The Rayleigh line and Hugoniot for air with initial pressure of 1 atm and initial temperature of 300 K. `demo_RH_air.m` (a) Frozen composition Hugoniot and Rayleigh line for a shock propagating at 1000 m/s. (b) Comparison of frozen and equilibrium composition Hugoniots and Rayleigh line for a shock propagating at 3500 m/s. `demo_RH_air_eq.m`

Entropy and Sound Speeds

According to (6.6), the entropy downstream of the shock wave must be greater than or equal to the entropy upstream. For nonreactive flow, this can be verified by computing the isentrope

$$s(P, v, \mathbf{Y}) = \text{constant} \quad (6.21)$$

with either fixed (frozen) composition $\mathbf{Y}_2 = \mathbf{Y}_1$ or shifting (equilibrium) composition $\mathbf{Y}_2 = \mathbf{Y}^{eq}(P, v)$. The slope of the isentrope can be interpreted in terms of the sound speed a

$$\left. \frac{\partial P}{\partial v} \right|_s = - \left(\frac{a}{v} \right)^2 \quad (6.22)$$

¹There is no strict rule about when dissociation begins to be significant. The extent of dissociation changes continuously with shock strength and is also dependent on pressure. The choice of 1000 m/s is arbitrary and chosen for convenience for this specific example.

Both the frozen (see MATLAB function `soundspeed.fr`)

$$a_f^2 = -v^2 \frac{\partial P}{\partial v} \Big|_{s, \mathbf{Y}} \quad (6.23)$$

and equilibrium (see MATLAB function `soundspeed_eq`)

$$a_e^2 = -v^2 \frac{\partial P}{\partial v} \Big|_{s, \mathbf{Y}^{eq}} \quad (6.24)$$

sound speeds are relevant for reacting flow computations. Frozen sound speeds are always slightly higher than equilibrium sound speeds in chemically reacting mixtures. Acoustic waves in chemically reacting flows are dispersive with the highest frequency waves traveling at the frozen sound speed and the lowest frequency waves traveling at the equilibrium sound speed (Vincenti and Kruger, 1965). The Python versions of the algorithms are defined as functions in `thermo.py`.

At low temperatures (<1000 K), there is little dissociation, and the difference between frozen and equilibrium isentropes or sound speeds is negligible. Further, the equilibrium algorithms used in Cantera have difficulty converging when a large number of species have very small mole fractions. This means that at low temperatures, it is often possible and necessary to only compute the frozen isentropes. Examples of the frozen isentropes (see the MATLAB script `demo_RH_air_isentropes.m`)

$$P = P(v, s) \Big|_{\mathbf{Y}} \quad (6.25)$$

are plotted on the P - v plane together with Hugoniot in Fig 6.4. The entropy for each isentrope is fixed at the value corresponding to the intersection of the isentrope and the Hugoniot. The isentrope labeled s_1 passes through the initial point 1 and the isentrope labeled s_4 passes through the shock state 2. The isentrope entropies are ordered as $s_4 > s_3 > s_2 > s_1$ in agreement with (6.6). Entropy increases along the Hugoniot.

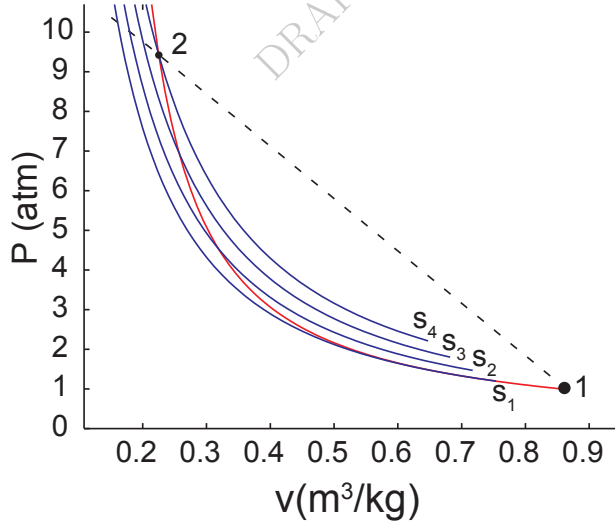


Figure 6.4: Frozen isentropes, Hugoniot, and a Rayleigh line for a 1000 m/s shock wave in air. `demo_RH_air_isentropes.m`

The graphical results for the relationship between Rayleigh lines and the isentropes illustrate a general principle for shock waves: the flow upstream is supersonic, the flow downstream is subsonic. At the initial state 1, the Rayleigh line is steeper than the isentrope

$$\frac{\partial P}{\partial v} \Big|_{s, \mathbf{Y}} > \frac{\Delta P}{\Delta v} \quad (6.26)$$

which from the definition of the slopes of the Rayleigh line (6.16) and isentrope (6.23) implies that the flow upstream of the wave is supersonic

$$w_1 > a_1 \quad (6.27)$$

At the final state 2, the isentrope is steeper than the Rayleigh line

$$\left. \frac{\partial P}{\partial v} \right|_{s, Y} < \frac{\Delta P}{\Delta v} \quad (6.28)$$

which implies that the flow downstream of the shock is subsonic (in the wave-fixed frame)

$$w_2 < a_2 \quad (6.29)$$

The isentrope is tangent to the Hugoniot at state 1 and also has the same curvature at this point so that weak shock waves are very close to acoustic waves (Thompson, 1972), with the entropy increasing like the cube of the volume change

$$\Delta s \propto |\Delta v|^3 \quad (6.30)$$

along the Hugoniot near point 1. The isentropes shown in Fig. 6.4 are frozen isentropes; in general, the correct choice of conditions (frozen vs equilibrium) for evaluating the isentropes depends on the end use.

See the following demos for frozen and equilibrium post shock states:

MATLAB: `demo_PSfr.m` and `demo_PSeq.m`

Python: `demo_PSfr.py` and `demo_PSeq.py`

6.5 Detonation Waves and the Chapman-Jouguet Condition

The Hugoniot for a stoichiometric hydrogen-air mixture and two example Rayleigh lines are shown in Figure 6.5. The possible solutions to the jump conditions are shown graphically as the intersection points of the Rayleigh lines and Hugoniot. On the upper (U) or detonation branch, the wave speed must be above some minimum value, the upper Chapman-Jouguet (CJ_U) velocity in order for there to be an intersection of the Rayleigh line and the detonation branch of the Hugoniot. On the lower (L) or deflagration branch, the wave speed must be less than some minimum value, the lower Chapman-Jouguet (CJ_L) velocity in order for there to be an intersection of the Rayleigh line and the detonation branch of the Hugoniot. If the perfect gas approximation is used, then it is possible to find analytic solutions (see Appendix A.3) for the Hugoniot and CJ states. For more general equations of state and realistic thermochemistry, it is necessary to use the numerical methods described in the subsequent sections. The purpose of this section is to present the theoretical background for the CJ state conditions used in those numerical methods.

The minimum pressure point on the detonation branch (CV) corresponds to the final state of a constant volume explosion. The maximum pressure point on the deflagration branch (CP) corresponds to the final state of a constant pressure explosion. Like shock waves, detonation waves are supersonic ($w_1 > a_1$) and a propagating wave will not induce flow upstream but only downstream. However, deflagration waves are subsonic ($w_1 < a_1$) and a propagating wave causes flow both upstream and downstream of the deflagration wave. Examples of deflagration waves in gases are low-speed flames. Since the flow upstream of the flame is subsonic, the flame propagation rate is strongly coupled to the fluid mechanics of the surrounding flow as well as the structure of the flame itself. This makes the deflagration solutions to the jump conditions much less useful than the detonation solutions since flame speeds cannot be determined uniquely by the jump conditions.

In general, there are two solutions (U_1, U_2) possible on the detonation branch for a given wave speed, $\infty > U > U_{CJ_U}$ and two solutions (L_1, L_2) possible on the lower (L) or deflagration branch for a given wave speed, $0 < U < U_{CJ_L}$. Only one of the two solutions is considered to be physically acceptable. These are the solution (U_1) for the detonation branch and the solution (L_2) for the deflagration branch. According

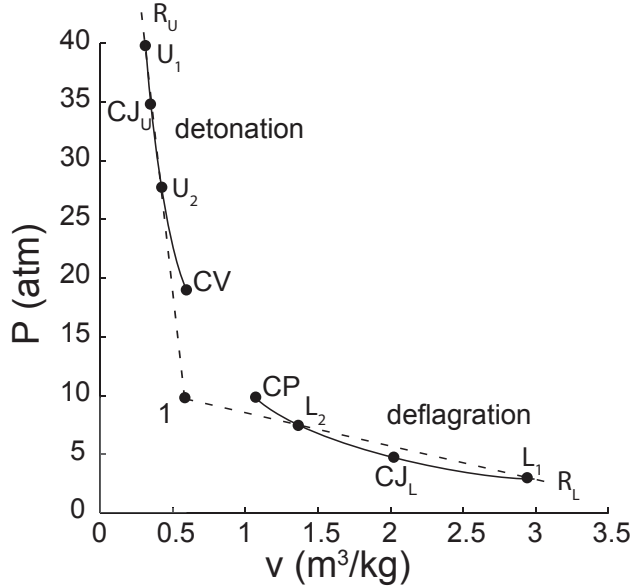


Figure 6.5: Equilibrium Hugoniot and two Rayleigh lines illustrating detonation and deflagration branches.

to Jouguet's rule (see Appendix C and Fickett and Davis (1979)), these solutions have subsonic flow behind the wave $w_2 < a_2$ and satisfy the condition of causality, which is that disturbances behind the wave can catch up to the wave and influence its propagation.

As first recognized by Chapman (1899), the geometry (Fig. 6.6) of the Hugoniot and Rayleigh line impose restrictions on the possible values of the detonation velocity. Below a minimum wave speed, $w_1 < w_{\text{CJ}}$, the Rayleigh line and equilibrium Hugoniot do not intersect and there are no steady solutions. For a wave traveling at the minimum wave speed $w_1 = U_{\text{CJ}}$, there is a single intersection with the equilibrium Hugoniot. Above this minimum wave speed $w_1 > U_{\text{CJ}}$, the Rayleigh line and equilibrium Hugoniot intersect at two points, usually known as the strong (S) and weak (W) solutions. Based on these observations, Chapman proposed that the measured speed of detonation waves corresponds to that of the minimum wave speed solution, which is unique. A more detailed description for determining the minimum wave speed is given in Appendix B. This leads to the following definition:

Definition I: *The Chapman-Jouguet detonation velocity is the minimum wave speed for which there exists a solution to the jump conditions from reactants to equilibrium products traveling at supersonic velocity.*

From the geometry (Fig. 6.6), it is clear that the minimum wave speed condition occurs when the Rayleigh line is tangent to the Hugoniot. The point of tangency is the solution for the equilibrium downstream state and is referred to as the CJ state, as indicated on Fig. 6.6. Jouguet (1905) showed that at the CJ point, the entropy is an extreme value and that as a consequence, the isentrope passing through the CJ point is tangent to the Hugoniot and therefore also tangent to the Rayleigh line as indicated in Figure 6.7 (see the MATLAB script demo_RH.CJ_isentropes.m). There are various ways to demonstrate this, e.g. differentiate (6.19) for a fixed initial state to obtain (dropping the subscript from state 2)

$$de = -\frac{1}{2} [\Delta v \, dP + (P + P_1) \, dv] \quad (6.31)$$

and combine this with the fundamental relation of thermodynamics

$$de = Tds - Pdv \quad (6.32)$$

to obtain

$$T \left. \frac{\partial s}{\partial v} \right|_{\mathcal{H}} = -\frac{\Delta v}{2} \left[\left. \frac{\partial P}{\partial v} \right|_{\mathcal{H}} - \frac{\Delta P}{\Delta v} \right] \quad (6.33)$$

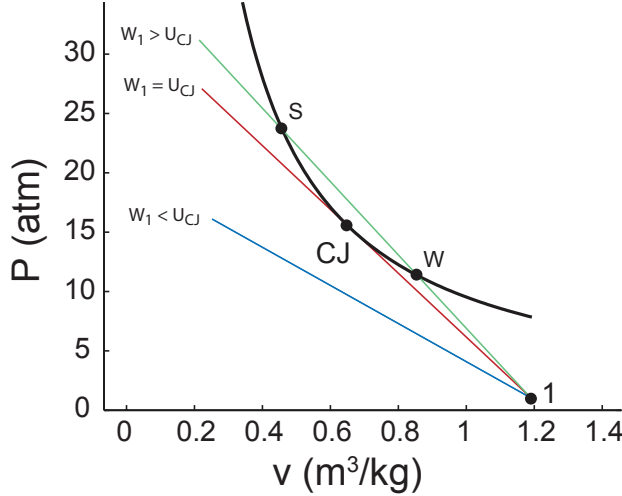


Figure 6.6: Hugoniot and three representative Rayleigh lines illustrating $w_1 = U_{CJ}$ as the minimum wave speed and tangency of Rayleigh line and Hugoniot at the CJ point.

where \mathcal{H} indicates a derivative evaluated on the Hugoniot. At the point of tangency between Rayleigh line and Hugoniot, the right hand side will vanish so that the entropy is an extremum at the CJ point.

$$\left. \frac{\partial s}{\partial v} \right|_{\mathcal{H}, CJ} = 0 \quad (6.34)$$

This implies that the isentrope passing through the CJ point must be tangent to the Rayleigh line and also the Hugoniot. The nature of the extremum can be determined by either algebraic computation of the curvature of the isentrope or geometric considerations. The entropy variation along the Hugoniot can be determined by inspecting the geometry of the isentropes and the Rayleigh lines. From the slopes shown in Fig. 6.7, we see that

$$\left. \frac{\partial s}{\partial v} \right|_{\mathcal{H}} < 0 \quad \text{for} \quad v < v_{CJ} \quad (6.35)$$

and

$$\left. \frac{\partial s}{\partial v} \right|_{\mathcal{H}} > 0 \quad \text{for} \quad v > v_{CJ} \quad (6.36)$$

so that the entropy is a local minimum at the CJ point.

$$\left. \frac{\partial^2 s}{\partial v^2} \right|_{\mathcal{H}, CJ} > 0 \quad (6.37)$$

The tangency of the isentrope to the Rayleigh lines at the CJ point

$$\frac{\Delta P}{\Delta v} = - \left(\frac{w_2}{v_2} \right)^2 = \left. \frac{\partial P}{\partial v} \right|_s = - \left(\frac{a_2}{v_2} \right)^2 \quad (6.38)$$

implies that

$$w_2 = a_2 \quad \text{at the CJ point.} \quad (6.39)$$

We conclude that at the CJ point, the flow in the products is moving at the speed of sound (termed *sonic* flow) relative to the wave. This leads to the alternative formulation (due to Jouguet) of the definition of the CJ condition.

Definition II: *The Chapman-Jouguet detonation velocity occurs when the flow in the products is sonic relative to the wave. This is equivalent to the tangency of the Rayleigh line, Hugoniot, and equilibrium isentrope at the CJ point.*

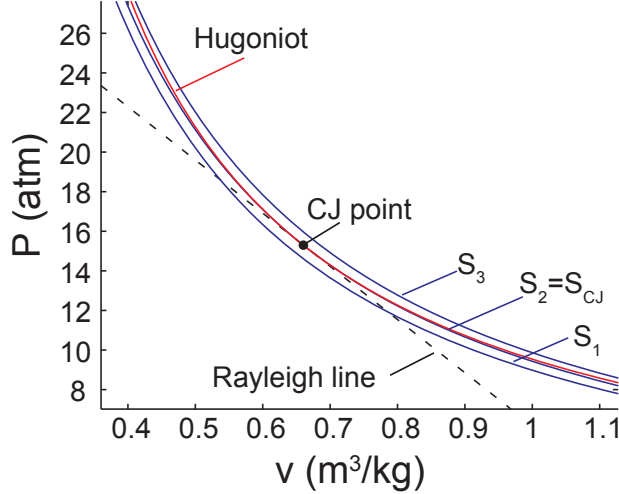


Figure 6.7: Hugoniot, Rayleigh line, and three representative isentropes (equilibrium) illustrating the tangency conditions at the CJ point. `demo_RH_CJ.isentropes.m`

The equilibrium isentrope and equilibrium sound speed appear in this formulation because the problem has been approached in a purely thermodynamic fashion with no consideration of time-dependence or detonation structure. In early studies, there was some controversy (see the discussion in [Wood and Kirkwood \(1959\)](#)) about the proper choice of sound speed, equilibrium vs. frozen. However, after careful examination of the equations of time-dependent reacting flow, see papers in [Kirkwood \(1967\)](#) and discussion in [Fickett and Davis \(1979\)](#), it became clear that a truly steady solution to the full reacting flow equations does not exist for most realistic models of reaction that include reversible steps. As a consequence, it is not possible to formulate a truly steady theory of detonation. A consistent thermodynamic theory will use the equilibrium sound speed to define the CJ point and this is what is used in our computations.

See the Following Examples - MATLAB: `demo_CJ.m` Python: `demo_CJ.py`

Physical Meaning of the CJ condition

The following heuristic argument is due to [Jouguet \(1905\)](#) and a mathematical version was first presented by [Brinkley and Kirkwood \(1949\)](#): Consider a detonation wave traveling faster than the CJ velocity such that the state behind the wave is the upper intersection (S – the strong solution) and the flow behind the wave is subsonic relative to the wave front. In this situation, perturbations from behind the detonation wave can propagate through the flow and interact with the leading shock. In particular, if the perturbations are expansion waves, these perturbations will eventually slow the lead shock to the CJ speed. Once the detonation is propagating at the CJ speed, the flow behind becomes sonic and acoustic perturbations can no longer affect the wave. Thus the CJ condition corresponds a self-sustained wave that is isolated from disturbances from the rear and can propagate indefinitely at the CJ speed. This is why detonation waves that have propagated over sufficiently long distances in tubes are observed to be close to the CJ velocity.

A similar argument cannot be made for the lower (W) or weak solution which has supersonic flow behind the wave relative to the wave front. From a theoretical viewpoint, for steady, planar wave the weak solution

is only accessible under very special circumstances that require a specific form of the reaction rate (see Chap. 5 of [Fickett and Davis, 1979](#)).

From an experimental viewpoint, the equilibrium CJ model gives reasonable values (within 1-2%) for detonation velocity under ideal conditions of initiation and confinement. However, this does not mean that the actual thermodynamic state corresponds to the CJ point (see Chap. 3 of [Fickett and Davis, 1979](#)) since the tangency conditions mean that the thermodynamic state is extremely sensitive to small variations in wave speed. Further, detonations in gases are unstable which leads to a three-dimensional front structure that cannot be eliminated in experimental measurements (see Chap. 7 of [Fickett and Davis, 1979](#)).

6.6 Reflected Waves

Assuming a known incident wave speed and upstream state, we can find the gas properties resulting from wave reflection at normal incidence on a rigid surface. We apply the normal shock jump conditions (Section 6.1) across both the incident and reflected waves to find the analog of the Rayleigh and Hugoniot equations. We use a frame of reference where the initial velocity of the reflecting surface has zero velocity. The upstream (1), post-incident-shock region (2), and post-reflected-shock region (3) are as shown in Fig. 6.8.

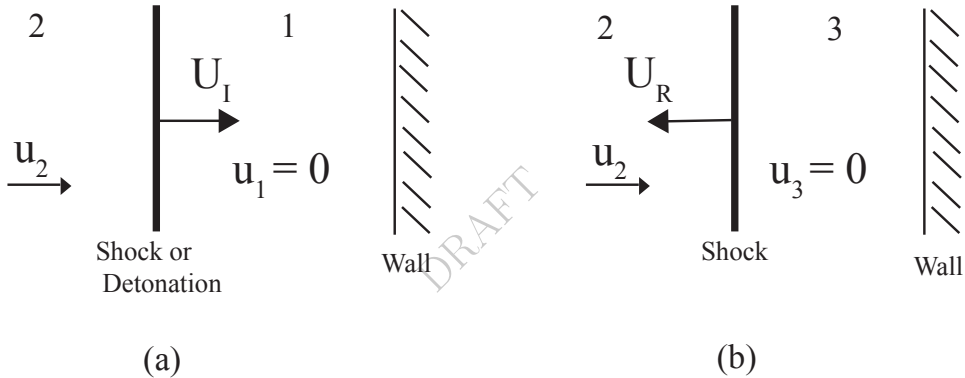


Figure 6.8: Diagrams showing the incident shock or detonation wave before (a) and after (b) reflection with a wall. States 1, 2, and 3 are shown.

Using the velocities in the wave fixed frame relative to the reflected shock for states 2 and 3 as shown in Fig. 6.8, we obtain the following wave-frame velocities for the reflected wave

$$w_2 = U_R + u_2 \quad (6.40)$$

$$w_3 = U_R \quad (6.41)$$

Substituting these into the usual shock jump conditions yields the following relationships across the reflected shock

$$(U_R + u_2)\rho_2 = U_R \rho_3 \quad (6.42)$$

$$P_2 + \rho_2(U_R + u_2)^2 = P_3 + \rho_3 U_R^2 \quad (6.43)$$

$$h_2 + \frac{1}{2}(U_R + u_2)^2 = h_3 + \frac{1}{2}U_R^2 \quad (6.44)$$

$$h_3 = h_3(P_3, \rho_3) \quad (6.45)$$

We combine these relationships in a manner similar to that used for incident shock waves to obtain equations for the shock speed

$$U_R = \frac{\frac{u_2}{\rho_3} - 1}{\frac{\rho_3}{\rho_2}}, \quad (6.46)$$

the pressure P_3 behind reflected shock

$$P_3 = P_2 + \frac{\frac{\rho_3 u_2^2}{\rho_3 - 1}}{\frac{\rho_3}{\rho_2}}, \quad (6.47)$$

and the enthalpy h_3 behind reflected shock

$$h_3 = h_2 + \frac{\frac{u_2^2}{2} \frac{\rho_3}{\rho_3 - 1} + 1}{\frac{\rho_3}{\rho_2}}. \quad (6.48)$$

For substances with realistic equations of state, these equations must be solved using an iterative numerical procedure. The numerical solution methods for reflected shock waves can be taken directly from those used for incident shock waves, which are described in subsequent sections. The post-incident-shock state (2) must be determined before the post-reflected-shock state (3) is found. If the perfect gas approximation is used, then it is possible to find analytic solutions (see Appendix A.2) for the conditions in the reflected region for a specified incident shock wave speed and initial state.

For the detonation wave case, the same procedure is repeated, but instead of an incident shock wave, the incident wave is a detonation and therefore reactive. The post-reflected-shock thermodynamic state (3) can either be considered in chemical equilibrium or frozen. Experimental, numerical, and approximate analytical solution methods for reflected detonations are compared in [Shepherd et al. \(1991\)](#).

See the following examples for equilibrium and frozen reflected post-shock states:

MATLAB: `demo_reflected_eq.m` and `demo_reflected_fr.m` Python: `demo_reflected_eq.py` and `demo_reflected_fr.py`

6.7 Relationship of Ideal Model parameters to Real Gas Properties

The two- γ model (Section A.3) contains six parameters ($R_1, \gamma_1, R_2, \gamma_2, q, U_{CJ}$ or M_{CJ}) that have to be determined from computations with a realistic thermochemical model and chemical equilibrium in the combustion products. This can be done with the programs described in the previous sections of this document.

The parameters are computed as follows:

$$R_1 = \frac{\mathcal{R}}{\mathcal{W}_1} \quad (6.49)$$

The universal gas constant (SI units) is

$$\mathcal{R} = 8314. \text{ J} \cdot \text{kmol}^{-1} \cdot \text{K}^{-1} \quad (6.50)$$

The mean molar mass is computed from the composition of the gas and the mixture formula

$$\mathcal{W} = \sum_{i=1}^K X_i \mathcal{W}_i \quad (6.51)$$

where X_i is the mole fraction of species i and \mathcal{W}_i is the molar mass of species i . The value of γ for the reactants can be interpreted as the ratio of the specific heats

$$\gamma_1 = \frac{C_{p,1}}{C_{v,1}} \quad (6.52)$$

This is identical to the logarithmic slope of the *frozen* isentrope

$$\gamma_{fr} = -\frac{v}{P} \left(\frac{\partial P}{\partial v} \right)_{s,fr} = \frac{a_{fr}^2}{Pv} \quad (6.53)$$

where the subscript *fr* indicates that the composition is held fixed or frozen. In order to compute the downstream state 2, we need to first find the CJ velocity which requires using software like the minimum velocity CJ algorithm `CJspeed` as in `demo.CJ.py` or `demo.CJ.m`.

Once the CJ conditions have been computed, the CJ state must be evaluated. This can be done using the jump condition solution algorithm `postshock_eq` with the computed CJ speed. This is implemented in the programs `demo.CJstate.py` and `demo.CJstate.m`. The CJ state includes the mean molar mass \mathcal{W}_2 and the value of the parameter γ_2 can be obtained from the logarithmic slope of the *equilibrium* isentrope.

$$\gamma_{eq} = -\frac{v}{P} \left(\frac{\partial P}{\partial v} \right)_{s,eq} \quad (6.54)$$

where the subscript *eq* implies that the derivative is carried out with shifting composition to maintain equilibrium. The value of the equilibrium sound speed can be used to find the numerical value of γ_{eq} .

$$\gamma_{eq} = \frac{a_{eq}^2}{Pv} \quad (6.55)$$

$$(6.56)$$

Once these parameters have been defined, the value of the parameter q can be obtained by solving the two- γ relationships (A.56), (A.57), and (A.58) to eliminate pressure, volume and temperature.

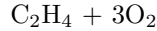
$$q = a_1^2 \left[\frac{(1 + \gamma_1 M_1^2)^2}{2(\gamma_2^2 - 1)} \left(\frac{\gamma_2}{\gamma_1} \right)^2 \frac{1}{M_1^2} - \frac{1}{\gamma_1 - 1} - \frac{M_1^2}{2} \right] \quad (6.57)$$

If the one- γ model is used, then this expression simplifies to

$$q = \frac{a_1^2}{2(\gamma^2 - 1)} \left(M_{CJ} - \frac{1}{M_{CJ}} \right)^2 \quad (6.58)$$

Example: Ethylene-Oxygen Detonation

A stoichiometric mixture of ethylene and oxygen has the composition



so that $X_{C2H4} = 0.25$ and $X_{O2} = 0.75$. The results of using the Cantera program `CJstate_isentrope` to compute the CJ velocity and state for initial conditions of 295 K and 1 bar are:

```
Initial pressure 100000 (Pa)
Initial temperature 295 (K)
Initial density 1.2645 (kg/m3)
a1 (frozen) 325.7368 (m/s)
gamma1 (frozen) 1.3417 (m/s)
```

```
Computing CJ state and isentrope for C2H4:1 O2:3.01 using gri30_highT.cti
CJ speed 2372.1595 (m/s)
CJ pressure 3369478.0035 (Pa)
CJ temperature 3932.4868 (K)
CJ density 2.3394 (kg/m3)
CJ entropy 11700.9779 (J/kg-K)
```

```
w2 (wave frame) 1282.1785 (m/s)
u2 (lab frame) 1089.9809 (m/s)
a2 (frozen) 1334.5233 (m/s)
a2 (equilibrium) 1280.6792 (m/s)
gamma2 (frozen) 1.2365 (m/s)
gamma2 (equilibrium) 1.1388 (m/s)
```

From the program output and gas objects computed by Cantera, we find the following parameters in Table 6.1

Table 6.1: Parameters for CJ detonation in stoichiometric ethylene-oxygen computed by the Shock and Detonation Toolbox.

\mathcal{W}_1	(kg/kmol)	31.0
a_1	(m/s)	325.7
γ_1		1.342
\mathcal{W}_2	(kg/kmol)	23.45
a_2	(m/s)	1280.
γ_2		1.139
U_{CJ}	(m/s)	2372.
M_{CJ}		7.28
q	(MJ/kg)	9.519

6.8 Inverse Shock Relations

The design and analysis of experiments often requires solving the inverse problem of finding a shock strength and upstream state (1) that corresponds to a given downstream stream state (2). For example, using a shock tube to create a specified reflected shock state requires working backward from a specified state at the end wall to compute the initial states in the driven and driver sections. In general, there is a locus of initial states $P_1(v_1)$ that corresponds to a specified final state (P_2, v_2) . This locus was termed the *inverse shock adiabat* by [Thompson and Sullivan \(1975\)](#).

The shock jump conditions, with the exception of the entropy condition, are symmetric. So any technique useful for solving the direct problem can be readily modified to solve the inverse problem. An approach that is useful not only for the inverse but also the direct approach is to work with the purely thermodynamic Hugoniot relationship in the pressure-volume plane. The inverse shock adiabat is set of solutions to the Hugoniot equation with specified downstream states.

$$\mathcal{H} : \quad h_1 = \textcolor{red}{h_2} - \frac{1}{2}(\textcolor{red}{P_2} - P_1)(\textcolor{red}{v_2} + v_1). \quad (6.59)$$

Given the downstream values (subscripts 2, highlighted in red), the goal is to solve for upstream values (subscripts 1). In order to do so, an equation of state in the form $h(P, v)$ is required. The dependence on composition has been suppressed and this formulation will work with either frozen or equilibrium states.

In the case of an ideal gas, $h = h(T)$ and $Pv = RT$ and we can compute the upstream and downstream states in terms of temperature and pressure. Substituting these relations into \mathcal{H}^i , we obtain the following quadratic equation for $P(T)$ in the upstream state

$$\left(\frac{P_1}{P_2}\right)^2 + \left[2\frac{h_2 - h_1(T_1)}{RT_2} + \frac{T_1}{T_2} - 1\right] \left(\frac{P_1}{P_2}\right) - \frac{T_1}{T_2} = 0. \quad (6.60)$$

The solution is

$$\frac{P_1}{P_2} = \sqrt{\left[\frac{h_2 - h_1(T_1)}{RT_2} + \frac{1}{2}\left(\frac{T_1}{T_2} - 1\right)\right]^2 + \frac{T_1}{T_2}} - \left[\frac{h_2 - h_1(T_1)}{RT_2} + \frac{1}{2}\left(\frac{T_1}{T_2} - 1\right)\right]. \quad (6.61)$$

For a perfect gas $h = C_P T$, $C_P = \gamma R / (\gamma - 1)$, the quadratic simplifies to

$$\left(\frac{P_1}{P_2}\right)^2 + \frac{\gamma + 1}{\gamma - 1} \left(1 - \frac{T_1}{T_2}\right) \left(\frac{P_1}{P_2}\right) - \frac{T_1}{T_2} = 0. \quad (6.62)$$

and the analytical solution is

$$\frac{P_1}{P_2} = \sqrt{\left[\frac{1}{2} \frac{\gamma + 1}{\gamma - 1} \left(1 - \frac{T_1}{T_2}\right)\right]^2 + \frac{T_1}{T_2}} - \left[\frac{1}{2} \frac{\gamma + 1}{\gamma - 1} \left(1 - \frac{T_1}{T_2}\right)\right]. \quad (6.63)$$

These results can be used to obtain solutions for the pressure ratio P_2/P_1 for either the direct (specified upstream state 1) or inverse problem (specified downstream state 2). The specific volume ratio can be computed from

$$\frac{v_1}{v_2} = \frac{T_1}{T_2} \sqrt{\frac{P_1}{P_2}}. \quad (6.64)$$

Upstream and downstream shock-relative velocities can be computed from the Rayleigh line relationship

$$\frac{w_1}{v_1} = \frac{w_2}{v_2} = \sqrt{-\frac{P_2 - P_1}{v_2 - v_1}} = \frac{P_2}{\sqrt{RT_2}} \sqrt{\frac{1 - P_1/P_2}{v_1/v_2 - 1}}, \quad (6.65)$$

The velocities can be computed from the downstream state, pressure, and volume ratios as

$$w_1 = \frac{v_1}{v_2} \sqrt{RT_2} \sqrt{\frac{1 - P_1/P_2}{v_1/v_2 - 1}}, \quad (6.66)$$

$$w_2 = \sqrt{RT_2} \sqrt{\frac{1 - P_1/P_2}{v_1/v_2 - 1}}. \quad (6.67)$$

The jump in velocity across the shock is

$$[u] = -[w] = \sqrt{(P_2 - P_1)(v_1 - v_2)} = \sqrt{RT_2} \sqrt{(1 - P_1/P_2)(v_1/v_2 - 1)} \quad (6.68)$$

These relationships are independent of the shock motion relative to the laboratory frame and can be used for either stationary or moving shock waves. In particular both an incident shock into a quiescent state or a reflected shock into a moving state can be treated with the appropriate transformation to shock-fixed coordinates.

In the perfect gas case, the solutions in terms of property ratios are dimensionless functions depending on the ratio of specific heats. If the velocities are expressed in terms of Mach numbers, then those relationships are also dimensionless.

$$M_1 = \frac{w_1}{a_1} = \frac{v_1}{v_2} \sqrt{\frac{1 - P_1/P_2}{v_1/v_2 - 1}} \frac{1}{\sqrt{\gamma T_1/T_2}}, \quad (6.69)$$

$$M_2 = \frac{w_2}{a_2} = \sqrt{\frac{1 - P_1/P_2}{v_1/v_2 - 1}} \frac{1}{\sqrt{\gamma}}. \quad (6.70)$$

Chapter 7

Applications

The functions in the toolbox can be combined and used together with other Cantera functions to solve a number of problems in shock and detonation physics. Notes and demonstration programs are provided for using this library to compute examples of normal and oblique shocks and detonations, shock and detonation tube operations, expansion waves, nozzle flows, ideal detonation and wave structure, propulsion systems and selected wave interaction problems. The demonstration programs are available in both MATLAB and Python versions.

7.1 Detonations in Tubes

The Chapman-Jouguet (CJ) model of an ideal detonation can be combined with the Taylor-Zeldovich (TZ) similarity solution (Taylor, 1950, Zel'dovich and Kompaneets, 1960) to obtain an analytic solution to the flow field behind a steadily-propagating detonation in a tube. The most common situation in laboratory experiments is that the detonation wave starts at the closed end of the tube and the gas in the tube is initially stationary, with flow velocity $u_1 = 0$. This solution can be constructed piecewise by considering the four regions shown on Figure 7.1; the stationary reactants ahead of the detonation mixture (state 1); the detonation wave between states 1 and 2; the expansion wave behind the detonation (between states 2 and 3); and the stationary products next to the closed end of the tube, state 3.

In this model, the detonation travels down the tube at a constant speed U , equal to the Chapman-Jouguet velocity U_{CJ} . The corresponding peak pressure, P_2 , is the Chapman-Jouguet pressure P_{CJ} . The structure of the reaction zone and the associated property variations such as the Von Neumann pressure spike are neglected in this model. The detonation wave instantaneously accelerates the flow and sets it into motion $u_2 > 0$, then the expansion wave gradually brings the flow back to rest, $u_3 = 0$. As an ideal detonation wave propagates through the tube, the expansion wave increases in width proportionally so that the flow always appears as shown in Fig. 7.1 with just a change in the scale of the coordinates. This is true only if we neglect non-ideal processes like friction and heat transfer that occur within the expansion wave. If the tube is sufficiently slender (length/diameter ratio sufficiently large), friction and heat transfer will limit the growth of the expansion wave.

Taylor-Zeldovich Expansion Wave

The properties within the expansion wave can be calculated by assuming a similarity solution with all properties a function $f(x/Ut)$. For a planar flow, the simplest method of finding explicit solutions is with the method of characteristics . There are two sets of characteristics, C^+ and C^- defined by

$$C^+ \quad \frac{dx}{dt} = u + a \quad (7.1)$$

$$C^- \quad \frac{dx}{dt} = u - a \quad (7.2)$$

$$(7.3)$$

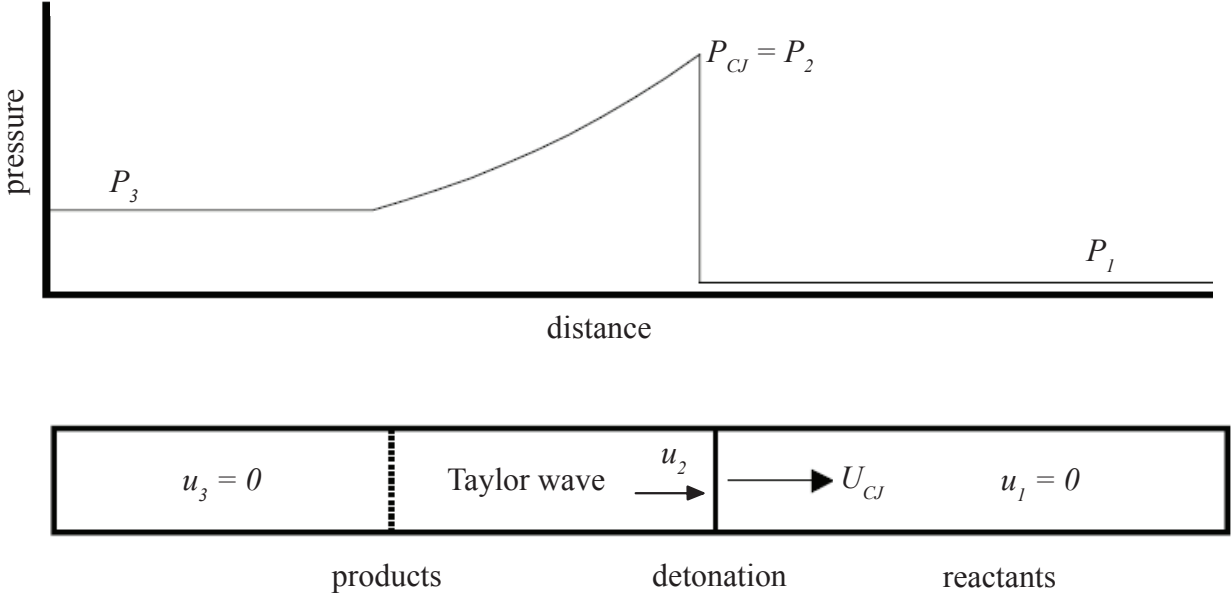


Figure 7.1: Detonation propagation in tube with a closed end.

On the characteristics the Riemann invariants J^\pm are defined and are constants in the smooth portions of the flow. In an ideal gas, the invariants are:

$$\text{on } C^+ \quad J^+ = u + F \quad (7.4)$$

$$\text{on } C^- \quad J^+ = u - F \quad (7.5)$$

$$(7.6)$$

The Riemann function F is defined as

$$F = \int_{P_\circ}^P \frac{dP'}{\rho a} \quad (7.7)$$

where P_\circ is a reference pressure and the integrand is computed along the isentrope s_\circ passing through states 2 and 3. For an ideal gas, the integral can be carried out and the indefinite integral is equal to

$$F = \frac{2a}{\gamma - 1} \quad (7.8)$$

In this section, the value of γ is everywhere taken to be the equilibrium value in the detonation products.

The solution proceeds by recognizing that within the expansion fan, $a_3 \geq x/t \geq U_{CJ}$, the C^+ characteristics are simply rays emanating from the origin of the $x-t$ coordinate system and between the end of the expansion fan and the wall, $0 \geq x/t \geq a_3$, the characteristics are straight lines.

$$\begin{aligned} \frac{dx}{dt} &= u + a = \frac{x}{t} & \text{for } a_3 < \frac{x}{t} < U_{CJ} \\ \frac{dx}{dt} &= a_3 & \text{for } 0 < \frac{x}{t} < a_3 . \end{aligned} \quad (7.9)$$

The characteristics C^- span the region between the detonation and the stationary gas and on these characteristics the Riemann invariant is constant. Evaluating the value at states 2 and 3 yields the value of the sound speed in region 3 given the state 2, the CJ condition.

$$J^- = u - \frac{2}{\gamma - 1} a = -\frac{2}{\gamma - 1} a_3 = u_2 - \frac{2}{\gamma - 1} a_2 . \quad (7.10)$$

From the CJ condition we have

$$u_2 = U_{\text{CJ}} - a_{\text{CJ}} . \quad (7.11)$$

and the sound speed in region 3 is

$$a_3 = \frac{\gamma + 1}{2} a_{\text{CJ}} - \frac{\gamma - 1}{2} U_{\text{CJ}} . \quad (7.12)$$

The variation of properties within the expansion wave can be determined using the similarity properties of the C^+ characteristics and the relationship between velocity and sound speed on the C^- characteristics within the expansion wave. The expansion fan is bounded by the C^+ characteristic at the tail of the expansion fan

$$C_{\text{tail}}^+ : \frac{dx}{dt} = a_3 , \quad (7.13)$$

and the detonation location which coincides with the head of the expansion fan

$$\text{Detonation: } \frac{dx}{dt} = U_{\text{CJ}} , \quad (7.14)$$

$$C_{\text{head}}^+ : \frac{dx}{dt} = u_2 + a_2 = U_{\text{CJ}} , \quad (7.15)$$

so that the expansion is within the region

$$a_3 t \leq x \leq U_{\text{CJ}} t . \quad (7.16)$$

The sound speed and velocity vary linearly with distance between the plateau region (state 3) and the detonation

$$\frac{a}{a_3} = 1 - \frac{\gamma - 1}{\gamma + 1} \left(1 - \frac{x}{a_3 t} \right) \quad a_3 t \leq x \leq U_{\text{CJ}} t \quad (7.17)$$

$$u = u_2 - \frac{2}{\gamma - 1} (a_2 - a) \quad a_3 t \leq x \leq U_{\text{CJ}} t \quad (7.18)$$

and are constant in the plateau region

$$a = a_3 \quad 0 \leq x \leq a_3 t \quad (7.19)$$

$$u = 0 \quad 0 \leq x \leq a_3 t \quad (7.20)$$

The other properties within the expansion fan can be found using the fact that the flow is isentropic in this region.

$$\frac{a}{a_3} = \left(\frac{T}{T_3} \right)^{\frac{1}{2}} \quad ; \quad \frac{P}{P_3} = \left(\frac{\rho}{\rho_3} \right)^{\gamma} \quad ; \quad \frac{T}{T_3} = \left(\frac{\rho}{\rho_3} \right)^{\gamma-1} \quad (7.21)$$

where T is the temperature, ρ is the density and P is the pressure. The state 3 can be computed from the CJ state values once a_3 is determined.

$$P_3 = P_{\text{CJ}} \left(\frac{a_3}{a_{\text{CJ}}} \right)^{\frac{2\gamma}{\gamma-1}} \quad (7.22)$$

$$T_3 = T_{\text{CJ}} \left(\frac{a_3}{a_{\text{CJ}}} \right)^{1/2} \quad (7.23)$$

$$\rho_3 = \rho_{\text{CJ}} \left(\frac{a_3}{a_{\text{CJ}}} \right)^{\frac{2}{\gamma-1}} \quad (7.24)$$

This finally gives for the pressure in the expansion wave

$$P = P_3 \left(1 - \left(\frac{\gamma - 1}{\gamma + 1} \right) \left[1 - \frac{x}{a_3 t} \right] \right)^{\frac{2\gamma}{\gamma-1}} \quad a_3 t \leq x \leq U_{\text{CJ}} t . \quad (7.25)$$

Determining Realistic TZ parameters

The states on the product isentrope need to be determined numerically, starting at the CJ point and extending to state 3. This is carried out in the program `demo_CJstate_isentrope` (**MATLAB**, **Python**) to numerically determine the value of thermodynamic properties such as density, sound speed, and temperature

$$\rho = \rho(P, s = s_{\text{CJ}}) \quad (7.26)$$

$$a = a(P, s = s_{\text{CJ}}) \quad (7.27)$$

$$T = T(P, s = s_{\text{CJ}}) \quad (7.28)$$

and also velocity in the TZ wave

$$u = u_2 + \int_{P_{\text{CJ}}}^P \frac{dP'}{(\rho a)_{s=s_{\text{CJ}}}} \quad (7.29)$$

parametrically as a function of pressure. The state 3 can be found by numerically solving the integral equation

$$u_2 = \int_{P_{\text{CJ}}}^{P_3} \frac{dP}{(\rho a)_{s=s_{\text{CJ}}}} \quad (7.30)$$

obtained by equating the Riemann invariant on the characteristic connecting states 2 and 3. In the program, the integral is carried out by using the trapezoidal rule with on the order of 100-200 increments on the isentrope. Interpolation is used to find state 3.

For the stoichiometric mixture of ethylene and oxygen discussed previously, the computation of state 3 using the Shock and Detonation Toolbox gives the following values.

Generating points on isentrope and computing Taylor wave velocity

State 3 pressure 1225686.0898 (Pa)

State 3 temperature 3608.3006 (K)

State 3 volume 1.0434 (m³/kg)

State 3 sound speed (frozen) 1253.7408 (m/s)

State 3 sound speed (equilibrium) 1201.0748 (m/s)

State 3 gamma frozen) 1.2291 (m/s)

State 3 gamma (equilibrium) 1.128 (m/s)

We note that there is a small change in γ_2 with the change in pressure on the isentrope and the pressure at state 3 is approximately $0.36P_{\text{CJ}}$.

7.2 Approximating the TZ Wave

The property variations within the ideal detonation wave are now completely specified. For example, the exact solution for the pressure profile is

$$P(x, t) = \begin{cases} P_1 & U_{\text{CJ}} < x/t < \infty \\ P_3 \left(1 - \left(\frac{\gamma-1}{\gamma+1}\right) \left[1 - \frac{x}{a_3 t}\right]\right)^{\frac{2\gamma}{\gamma-1}} & a_3 < x/t < U_{\text{CJ}} \\ P_3 & 0 < x/t < a_3 \end{cases} \quad (7.31)$$

In analytical studies, it is useful to approximate the dependence of the pressure within the expansion wave with a simpler function. Experimenting with several functional forms ([Beltman and Shepherd, 2002](#)) shows that an exponential can be used to represent this variation. At a fixed point in space, the variation of pressure with time can be represented by

$$P(x, t) = \begin{cases} P_1 & 0 < t < t_{\text{CJ}} \\ (P_2 - P_3) \exp(-(t - t_{\text{CJ}})/T) + P_3 & t_{\text{CJ}} < t < \infty \end{cases} \quad (7.32)$$

Where $t_{\text{CJ}} = x/U_{\text{CJ}}$ is the time it takes for a detonation to travel from the origin to the measurement location x . The time constant T can be determined by fitting the exponential relationship to the exact expression. The exact expression for pressure in the expansion wave can be rewritten as

$$P(x, t) = P_3 \left[1 - \frac{\gamma - 1}{\gamma + 1} \left(\frac{U_{\text{CJ}}/c_3 - 1 - \tau/t_{\text{CJ}}}{1 + \tau/t_{\text{CJ}}} \right) \right]^{\frac{2\gamma}{\gamma - 1}} \quad (7.33)$$

where $\tau = t - t_{\text{CJ}}$. By inspection of the argument in the exact expression, we see that the time constant should have the form

$$T = \alpha_T t_{\text{CJ}} \quad (7.34)$$

The constant α_T is a function of the ratio of specific heats γ and the parameter U_{CJ}/a_3 . Computations of these parameters using the one- γ model shows that $1.9 < a_3/U_{\text{CJ}} < 2$ for a wide range of values of γ and detonation Mach numbers $5 < M_{\text{CJ}} < 10$. Fitting the exponential function to the pressure variation in the expansion wave for this range of parameters yields a $0.31 < \alpha_T < 0.34$. A useful approximation is

$$T \approx \frac{t_{\text{CJ}}}{3} \quad (7.35)$$

In actual practice, if we are trying to represent the variation of pressure over a limited portion of a detonation tube, it is sufficient to take T to be a constant and this can be evaluated at some intermediate location within the portion of the tube that is of interest. For example, the middle of the center section of the Caltech 280-mm diameter detonation tube is about 4 m from the initiator. A detonation traveling 1500 m/s takes approximately 2.7 ms to reach this point and the characteristic decay time $T \approx 0.9$ ms.

Comparison of Two-Gamma and Real gas models

For the stoichiometric ethylene-oxygen example discussed in the text, the two- γ and real gas results are compared in detail in Table 7.1.

Table 7.1: Comparison of real gas and two- γ results for a CJ detonation in stoichiometric ethylene-oxygen.

Parameter	SD Toolbox Value	2- γ Model
M_{CJ}	7.282	7.287
P_2/P_1	33.69	33.78
ρ_2/ρ_1	1.850	1.852
T_2/T_1	13.33	13.80
a_3 (m/s)	1201.1	1206.2
P_3 (MPa)	1.225	1.242
T_3 (K)	3608.3	3603.0
ρ_3	0.9584	0.9726

7.3 Oblique Waves

An oblique shock or detonation wave can be treated using the methods developed for planar one-dimensional waves with a geometrical transformation and recognizing that only the component of velocity normal to the wave changes and the velocity component tangential to the wave is unchanged across a shock or detonation wave. This is equivalent to transforming to a coordinate system with an orthogonal set of axes in which the wave lies along one of the axes. Only the component of velocity perpendicular or *normal* to the wave plays a role in the solution to the jump conditions. From the geometry of Fig. 7.2, the equations for the upstream and downstream normal velocity components are related to the net velocities $u = \sqrt{w^2 + v^2}$ upstream and

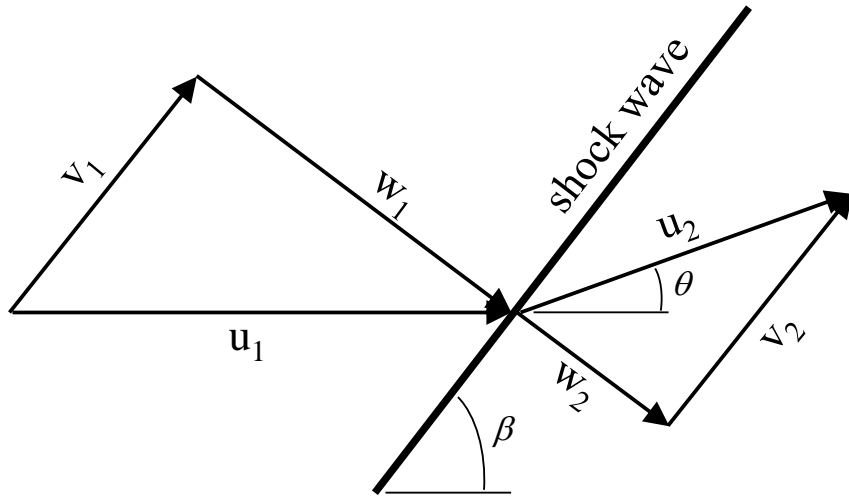


Figure 7.2: Geometry of oblique shock or detonation illustrating normal and perpendicular components

downstream of the wave by:

$$w_1 = u_1 \sin \beta \quad (7.36)$$

$$w_2 = u_2 \sin(\beta - \theta) \quad (7.37)$$

Where β is the detonation wave angle, and θ is the flow deflection angle. For shock waves, the upstream normal velocity component w_1 is always supersonic so that $w_1 \geq a_1$ and for detonation waves, the upstream normal velocity component has to be equal to or greater than or equal to the CJ value, $w_1 \geq w_{CJ}$. The tangential components of velocity,

$$v_1 = u_1 \cos \beta \quad (7.38)$$

$$v_2 = u_2 \cos(\beta - \theta) \quad (7.39)$$

are constant across the wave, $v_1 = v_2$ which implies that:

$$w_2 = u_1 \cos \beta \tan(\beta - \theta)$$

Combining this last relation with the geometric transformations and the solutions to the normal shock or detonation wave jump conditions, the wave angle β and the flow deflection angle θ can be determined for a given upstream velocity u_1 and normal velocity w_1 by using elementary trigonometric function relationships:

$$\beta = \sin^{-1}(w_1/u_1) \quad (7.40)$$

$$\theta = \beta - \tan^{-1} \left(\frac{w_2}{\sqrt{u_1^2 - w_1^2}} \right) \quad (7.41)$$

The velocity w_2 required for finding θ is determined by the solution of the jump conditions for the specified upstream conditions and normal velocity w_1 ,

$$\rho_1 w_1 = \rho_2 w_2 \quad (7.42)$$

$$P_1 + \rho_1 w_1^2 = P_2 + \rho_2 w_2^2 \quad (7.43)$$

$$h_1 + \frac{1}{2} w_1^2 = h_2 + \frac{1}{2} w_2^2 \quad (7.44)$$

The other thermodynamic properties downstream of the wave (state 2) are also given by the solution to these jump conditions. In terms of the angles β and θ , the downstream states can be expressed as:

$$\frac{\rho_2}{\rho_1} = \frac{\tan \beta}{\tan(\beta - \theta)} \quad (7.45)$$

$$\frac{[w]}{a_1} = -\frac{M_1^2 \sin^2 \theta}{\cos \beta (1 + \tan \beta \tan \theta)} \quad (7.46)$$

$$\frac{[P]}{\rho_1 a_1^2} = \frac{M_1^2 \tan \theta}{\cos \beta + \tan \theta} \quad (7.47)$$

In the case of perfect gases (constant specific heat), these equations can be solved analytically for relationships between the thermodynamic property changes, β and θ as discussed in Appendix A.9. The normal velocity component has to be selected from within the physically possible range of values:

$$\text{Shock waves: } u_1 \geq w_1 \geq a_1 \quad (7.48)$$

$$\text{Detonation waves: } u_1 \geq w_1 \geq U_{\text{CJ}} \quad (7.49)$$

where U_{CJ} is the Chapman-Jouguet velocity computed for the upstream state 1. These limits and the trigonometry of the velocity components imply that the wave angles are also limited in range:

$$\text{Shock waves: } \frac{\pi}{2} \geq \beta \geq \sin^{-1} \frac{1}{M_1} \quad (7.50)$$

$$\text{Detonation waves: } \frac{\pi}{2} \geq \beta \geq \sin^{-1} \frac{1}{M_{\text{CJ}}} \quad (7.51)$$

where $M_1 = u_1/a_1$ and $M_{\text{CJ}} = U_{\text{CJ}}/a_1$. The flow deflection angle is a multi-valued function of the wave angle or downstream thermodynamic state. This has significant implications for the shock and detonation wave configurations and interactions. The deflection angle θ has a maximum value for both detonations and shock waves. There is no minimum deflection angle for oblique shock waves, $\theta_{\min} = 0$ at both $\beta = \beta_{\min}$ and $\pi/2$. For oblique detonation wave, θ has a nonzero value at β_{CJ} and is zero at $\beta = \pi/2$. The maximum flow deflection angle must in general be computed numerically. One way to go about this is by computing the analytical expression for the derivative of the flow deflection angle with respect to the upstream normal velocity. A numerical root-solver can then be used to solve for the value of the upstream normal velocity which makes this derivative zero.

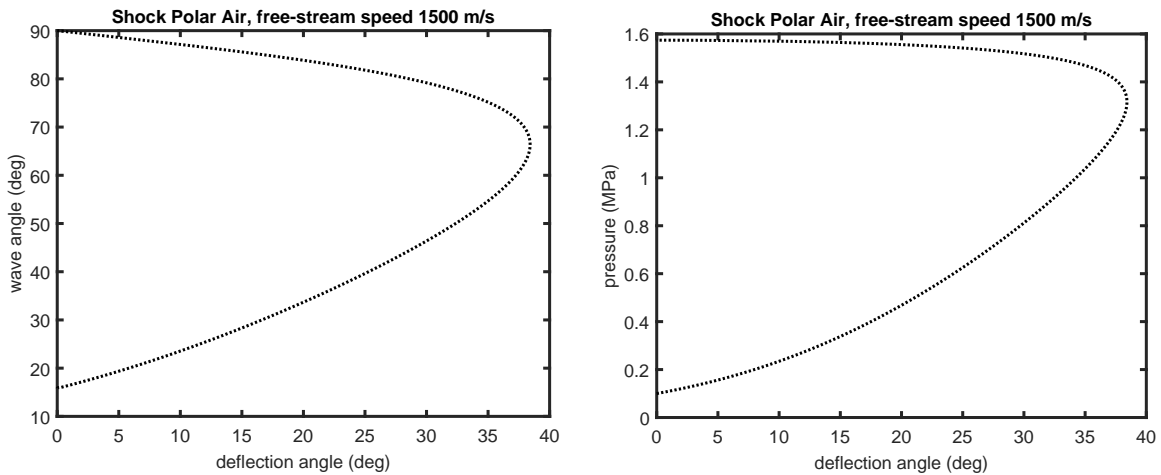


Figure 7.3: Examples of shock polars for air computed with frozen composition using [demo_oblique.m](#).

The results of either numerical or analytic computations can be usefully represented as *polar curves*, for example post-shock pressure *vs* flow deflection $P(\theta)$ or wave angle as a function of flow deflection $\beta(\theta)$, see